Published for SISSA by Springer

Received: October 19, 2012
Accepted: December 11, 2012
Published: January 9, 2013

Higgs bosons at 98 and 125 GeV at LEP and the LHC

Geneviève Bélanger,[a] **Ulrich Ellwanger,**[b] **John F. Gunion,**[c] **Yun Jiang,**[c] **Sabine Kraml**[d] **and John H. Schwarz**[e]

[a] *LAPTH, Université de Savoie, CNRS, B.P.110, F-74941 Annecy-le-Vieux Cedex, France*
[b] *Laboratoire de Physique Théorique, Université Paris-Sud, Centre d'Orsay, F-91405 Orsay-Cedex, France*
[c] *Department of Physics, University of California, Davis, CA 95616, U.S.A.*
[d] *Laboratoire de Physique Subatomique et de Cosmologie, UJF Grenoble 1, CNRS/IN2P3, INPG, 53 Avenue des Martyrs, F-38026 Grenoble, France*
[e] *Department of Physics, California Institute of Technology, Pasadena, CA 91125, U.S.A.*

E-mail: belanger@lapp.in2p3.fr, Ulrich.Ellwanger@th.u-psud.fr, jfgunion@ucdavis.edu, yunjiang@ucdavis.edu, sabine.kraml@lpsc.in2p3.fr, jhs@theory.caltech.edu

Abstract: We discuss NMSSM scenarios in which the lightest Higgs boson h_1 is consistent with the small LEP excess at ~ 98 GeV in $e^+e^- \to Zh$ with $h \to b\bar{b}$ and the heavier Higgs boson h_2 has the primary features of the LHC Higgs-like signals at 125 GeV, including an enhanced $\gamma\gamma$ rate. Verification or falsification of the 98 GeV h_1 may be possible at the LHC during the 14 TeV run. The detection of the other NMSSM Higgs bosons at the LHC and future colliders is also discussed, as well as dark matter properties of the scenario under consideration.

Keywords: Higgs Physics, Beyond Standard Model

ArXiv ePrint: 1210.1976

doi:10.1007/JHEP01(2013)069

JHEP01(2013)069

Contents

JHEP01(2013)069

1 Introduction

Data from the ATLAS and CMS collaborations [1, 2] provide an essentially 5σ signal for a Higgs-like resonance, h, with mass of order 125 GeV. Meanwhile, the CDF and D0 experiments have announced new results [3], based mainly on Vh associated production with $h \to b\bar{b}$, that support the ~ 125 GeV Higgs-like signal. While it is certainly possible that the observed signals in the various production/decay channels will converge towards their respective Standard Model (SM) values, the current central values for the signal strengths in individual channels deviate by about 1–2 σ from predictions for the $h_{\rm SM}$. One of the most significant deviations in the current data is the enhancement in the $\gamma\gamma$ final state for both gluon fusion (gg) and vector boson fusion (VBF) production. Such a result is not atypical of models with multiple Higgs bosons in which the $b\bar{b}$ partial width of the observed h is reduced through mixing with a second (not yet observed at the LHC) Higgs boson, h', thereby enhancing the $\gamma\gamma$ branching ratio of the h [4–9]. In such models, a particularly interesting question is whether one could simultaneously explain the LHC signal and the small ($\sim 2\sigma$) LEP excess in $e^+e^- \to Zb\bar{b}$ in the vicinity of $M_{b\bar{b}} \sim 98$ GeV [10, 11] using the h' with $m_{h'} \sim 98$ GeV. We recall that the LEP excess is clearly inconsistent with a SM-like Higgs boson at this mass, being only about $10-20\%$ of the rate predicted for the $h_{\rm SM}$. Consistency with such a result for the h' is natural if the h' couples at a reduced level to ZZ, which, in turn, is automatic if the h has substantial ZZ coupling, as required by the observed LHC signals.

In this paper we demonstrate that the two lightest CP-even Higgs bosons,[1] h_1 and h_2, of the Next-to-Minimal Supersymmetric Model (NMSSM) could have properties such that the h_1 fits the LEP excess at ~ 98 GeV while the h_2 is reasonably consistent with the Higgs-like LHC signals at ~ 125 GeV, including in particular the larger-than-SM signal in the $\gamma\gamma$ channel. The NMSSM [12] is very attractive since it solves the μ problem of the minimal supersymmetric extension of the SM (MSSM): the ad hoc parameter μ appearing in the MSSM superpotential term $\mu\hat{H}_u\hat{H}_d$ is generated in the NMSSM from the $\lambda\hat{S}\hat{H}_u\hat{H}_d$ superpotential term when the scalar component S of $\hat{S}$ develops a VEV $\langle S\rangle = s$: $\mu_{\rm eff} = \lambda s$. The three CP-even Higgs fields, contained in H_u, H_d and S, mix and yield the mass eigenstates h_1, h_2 and h_3. A 125 GeV Higgs state with enhanced $\gamma\gamma$ signal rate is easily obtained for large λ and small $\tan\beta$ [5] (see also [7, 8]). To describe the LEP and LHC data the h_1 and h_2 must have $m_{h_1} \sim 98$ GeV and $m_{h_2} \sim 125$ GeV, respectively, with the h_1 being largely singlet and the h_2 being primarily doublet (mainly H_u for the scenarios we consider). In addition to the CP-even states, there are also two CP-odd states, a_1 and a_2, and a charged Higgs boson, $H^\pm$. Verification of the presence of the three CP-even Higgs bosons and/or two CP-odd Higgs bosons would establish a Higgs field structure that goes beyond the two-doublet structure of the MSSM.

2 Higgs boson production and decay

The main production/decay channels relevant for current LHC data are gluon fusion (gg) and vector boson fusion (VBF) with Higgs decay to $\gamma\gamma$ or $ZZ^* \to 4\ell$. The LHC also probes W, Z+Higgs with Higgs decay to $b\bar{b}$, a channel for which Tevatron data is relevant, and WW →Higgs with Higgs→ $\tau^+\tau^-$. We compute the ratio of the gg or VBF induced Higgs cross section times the Higgs branching ratio to a given final state X, relative to the corresponding value for the SM Higgs boson, as

$$R^{h_i}_{gg}(X) \equiv \frac{\Gamma(h_i \to gg)\ \mathrm{BR}(h_i \to X)}{\Gamma(h_{\rm SM} \to gg)\ \mathrm{BR}(h_{\rm SM} \to X)}, \quad R^{h_i}_{\rm VBF}(X) \equiv \frac{\Gamma(h_i \to WW)\ \mathrm{BR}(h_i \to X)}{\Gamma(h_{\rm SM} \to WW)\ \mathrm{BR}(h_{\rm SM} \to X)}, \tag{2.1}$$

where h_i is the i^{th} NMSSM scalar Higgs, and $h_{\rm SM}$ is the SM Higgs boson, taking $m_{h_{\rm SM}} = m_{h_i}$. In the context of any two-Higgs-doublet plus singlets model, not all the R^{h_i} are independent. For example, $R^{h_i}_{VH}(X) = R^{h_i}_{VBF}(X)$, $R^{h_i}_{Y}(\tau\tau) = R^{h_i}_{Y}(bb)$[2] and $R^{h_i}_{Y}(ZZ) = R^{h_i}_{Y}(WW)$. A complete independent set of R^{h_i}'s can be taken to be (with $h = h_1$ or $h = h_2$)

$$R^h_{gg}(WW), \quad R^h_{gg}(bb), \quad R^h_{gg}(\gamma\gamma), \quad R^h_{VBF}(WW), \quad R^h_{VBF}(bb), \quad R^h_{VBF}(\gamma\gamma)\,. \tag{2.2}$$

In order to display the ability of the NMSSM to simultaneously explain the LEP and LHC Higgs-like signals, we turn to NMSSM scenarios with semi-unified GUT scale soft-SUSY-breaking. By "semi-unified" we mean universal gaugino mass parameter $m_{1/2}$, scalar

[1] We assume absence of CP-violating phases in the Higgs sector.

[2] This equality is altered by radiative corrections at large $\tan\beta$; however, these are small in our scenarios all of which have small to moderate $\tan\beta$ values.

JHEP01(2013)069

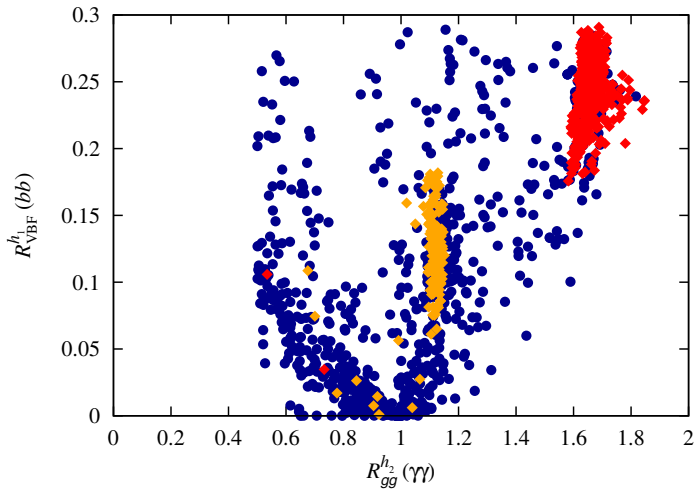

Figure 1. Signal strengths (relative to SM) $R^{h_1}_{VBF}(bb)$ versus $R^{h_2}_{gg}(\gamma\gamma)$ for $m_{h_1} \in [96, 100]$ GeV and $m_{h_2} \in [123, 128]$ GeV. In this and all subsequent plots, points with $\Omega h^2 < 0.094$ are represented by blue circles and points with $\Omega h^2 \in [0.094, 0.136]$ (the "WMAP window") are represented by red/orange diamonds.

(sfermion) mass parameter m_0, and trilinear coupling $A_0 \equiv A_t = A_b = A_\tau$ at the GUT scale, but $m^2_{H_u}$, $m^2_{H_d}$ and m^2_S as well as A_λ and A_κ are taken as non-universal at $M_{\rm GUT}$. Specifically, we use points from scans performed using NMSSMTools 3.2.0 [13–15], which includes the scans of [8] supplemented by additional runs following the same procedure as well as specialized MCMC chain runs designed to focus on parameter regions of particular interest. All the accepted points correspond to scenarios that obey all experimental constraints (mass limits and flavor constraints as implemented in NMSSMTools, $\Omega h^2 < 0.136$ and 2011 XENON100 constraints on the spin-independent scattering cross section) except that the SUSY contribution to the anomalous magnetic moment of the muon, δa_μ, is too small to explain the discrepancy between the observed value of a_μ [16] and that predicted by the SM. For a full discussion of the kind of NMSSM model employed see [7, 8, 17].

We first display in figure 1 the crucial plot that shows $R^{h_1}_{VBF}(bb)$ versus $R^{h_2}_{gg}(\gamma\gamma)$ when $m_{h_1} \in [96, 100]$ GeV and $m_{h_2} \in [123, 128]$ GeV are imposed in addition to the above mentioned experimental constraints.[3] (In this and all subsequent plots, points with $\Omega h^2 < 0.094$ are represented by blue circles and points with $\Omega h^2 \in [0.094, 0.136]$ (the "WMAP window") are represented by red and orange diamonds. These two colors are associated with different LSP masses as will be discussed below.) Note that $R^{h_1}_{VBF}(bb)$ values are required to be smaller than 0.3 by virtue of the fact that the LEP constraint on the $e^+e^- \to Zb\bar{b}$ channel with $M_{b\bar{b}} \sim 98$ GeV is included in the NMSSMTools program. Those points with $R^{h_1}_{VBF}(bb)$ between about 0.1 and 0.25 would provide the best fit to the LEP excess. (We note again that $R^{h_1}_{VBF}(bb)$ is equivalent to $R^{h_1}_{Vh_1}(bb)$ as relevant for LEP.) A large portion of such points have $R^{h_2}_{gg}(\gamma\gamma) > 1$ as preferred by LHC data. In

[3] Here the Higgs mass windows are designed to allow for theoretical errors in the computation of the Higgs masses.

JHEP01(2013)069

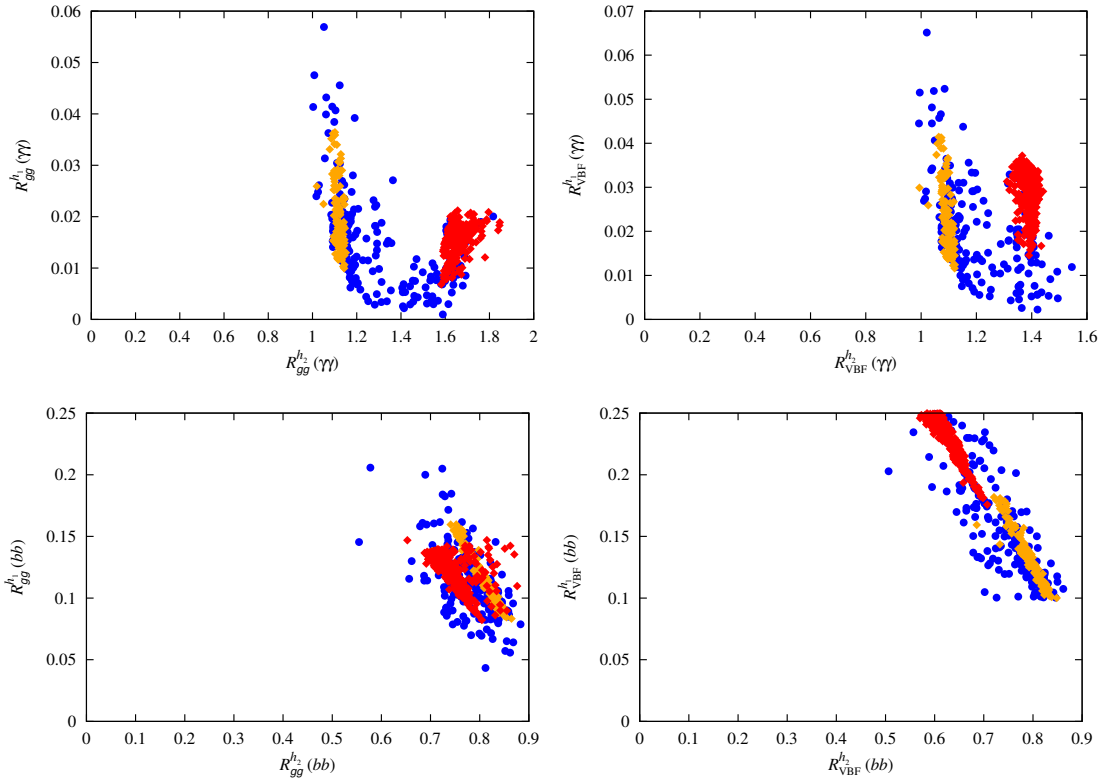

Figure 2. For the h_1 and h_2, we plot (top) $R^h_{gg}(\gamma\gamma)$ and $R^h_{VBF}(\gamma\gamma)$ and (bottom) $R^h_{gg}(bb)$ and $R^h_{VBF}(bb)$ for NMSSM scenarios consistent with the LEP and LHC Higgs excesses. More specifically, in this and all subsequent plots we only show points that satisfy all the basic constraints specified in the text and that also satisfy $m_{h_1} \in [96, 100]$ GeV, $m_{h_2} \in [123, 128]$ GeV, $R^{h_2}_{gg}(\gamma\gamma) > 1$ and $R^{h_1}_{VBF}(bb) \in [0.1, 0.25]$. These we have termed the "98 + 125 GeV Higgs scenarios". Regarding the WMAP-window points, we refer to the red diamonds as "region A" and to the orange ones as "region B".

all the remaining plots we will impose the additional requirements: $R^{h_2}_{gg}(\gamma\gamma) > 1$ and $0.1 \leq R^{h_1}_{VBF}(bb) \leq 0.25$. In the following, we will refer to these NMSSM scenarios as the "98 + 125 GeV Higgs scenarios". To repeat, the $R^{h_2}_{gg}(\gamma\gamma) > 1$ requirement is such as to focus on points that could be consistent (within errors) with the enhanced $\gamma\gamma$ Higgs signal at the LHC of order 1.5 times the SM. The $0.1 \leq R^{h_1}_{VBF}(bb) \leq 0.25$ window is designed to reproduce the small excess seen in LEP data at $M_{b\bar{b}} \sim 98$ GeV in the $Zb\bar{b}$ final state.

In figure 2, we plot (upper row) $R^{h_1}_{gg}(\gamma\gamma)$ vs. $R^{h_2}_{gg}(\gamma\gamma)$ and $R^{h_1}_{VBF}(\gamma\gamma)$ vs. $R^{h_2}_{VBF}(\gamma\gamma)$ and (lower row) $R^{h_1}_{gg}(bb)$ vs. $R^{h_2}_{gg}(bb)$ and $R^{h_1}_{VBF}(bb)$ vs. $R^{h_2}_{VBF}(bb)$. In these and all subsequent plots, we only show points that satisfy all the basic constraints specified earlier and that also satisfy $m_{h_1} \in [96, 100]$ GeV, $m_{h_2} \in [123, 128]$ GeV, $R^{h_2}_{gg}(\gamma\gamma) > 1$ and $R^{h_1}_{VBF}(bb) \in [0.1, 0.25]$. The upper plots show that the h_2 can easily have an enhanced $\gamma\gamma$ signal for both gg and VBF production whereas the $\gamma\gamma$ signal arising from the h_1 for both production mechanisms is quite small and unlikely to be observable. Note the two different $R^{h_2}_{gg}(\gamma\gamma)$ regions for which Ωh^2 lies in the WMAP window, one with $R^{h_2}_{gg}(\gamma\gamma) \sim 1.6$ (region A, red diamonds) and the other with $R^{h_2}_{gg}(\gamma\gamma) \sim 1.1$ (region B, orange diamonds). As we will show later,

JHEP01(2013)069

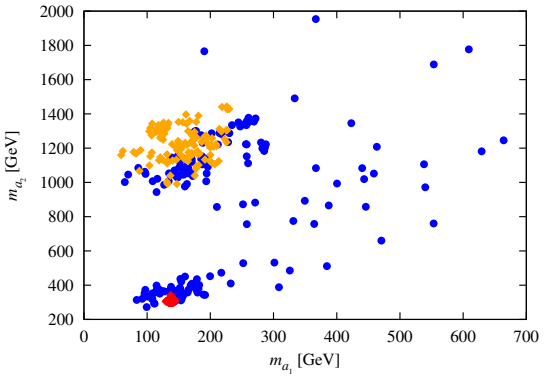

Figure 3. Scatter plot of m_{a_2} versus m_{a_1} for the 98+125 GeV scenario; note that $m_{a_2} \simeq m_{h_3} \simeq m_{H^\pm}$. Note that in this figure there is a dense region, located at $(m_{a_1}, m_{a_2}) \sim (130, 330)$ GeV, of strongly overlapping red diamond points. These are the points associated with the low-$m_{\widetilde{\chi}_1^0}$ WMAP-window region of parameter space. Corresponding dense regions appear in figures 4–7 and 10.

region A corresponds to $m_{\widetilde{\chi}_1^0} \sim 77$ GeV and $m_{\tilde{t}_1}$ between 197 GeV and 1 TeV, while the region B corresponds to $m_{\widetilde{\chi}_1^0} > 93$ GeV and $m_{\tilde{t}_1} > 1.8$ TeV. These same two regions will emerge in many subsequent figures. If $R^{h_2}_{gg}(\gamma\gamma)$ ends up converging to a large value, then masses for all strongly interacting SUSY particles would be close to current limits if the present $98 + 125$ GeV LEP-LHC Higgs scenario applies.

The bottom row of the figure focuses on the $b\bar{b}$ final state. We observe the reduced $R^{h_2}_{gg}(bb)$ and $R^{h_2}_{VBF}(bb)$ values that are associated with reduced $b\bar{b}$ width (relative to the SM) needed to have enhanced $R^{h_2}_{gg}(\gamma\gamma)$ and $R^{h_2}_{VBF}(\gamma\gamma)$. Meanwhile, the $R^{h_1}_{gg}(bb)$ and $R^{h_1}_{VBF}(bb)$ values are such that the h_1 could not yet have been seen at the Tevatron or LHC. Sensitivity to $R^{h_1}_{gg}(bb)$ ($R^{h_1}_{VBF}(bb)$) values from 0.05 to 0.2 (0.1 to 0.25) will be needed at the LHC. This compares to expected sensitivities after the $\sqrt{s} = 8$ TeV run in these channels to R values of at best 0.8.[4] Statistically, a factor of 4 to 10 improvement requires integrated luminosity of order 16 to 100 times the current $L = 10$ fb^{-1}. Such large L values will only be achieved after the LHC is upgraded to 14 TeV, although we should note that the luminosity required to probe this signal at 14 TeV could be lower than indicated by this simple estimate as the sensitivity to the Higgs signal improves at higher energies. Finally, the reader should note that for WMAP-window points the largest $R^{h_1}_{VBF}(bb)$ values occur for region A described above for which supersymmetric particle masses are as small as possible.

3 Other NMSSM particles and parameters

It is also very interesting to consider expectations for the other NMSSM particles in these scenarios. For this purpose, we present a series of plots. figure 3 displays the pseudoscalar masses in the m_{a_1}–m_{a_2} plane. We do not plot m_{h_3} nor $m_{H^\pm}$ since their masses are such that

[4]Here, we have used figure 12 of [2] extrapolated to a Higgs mass near 98 GeV and assumed $L = 20$ fb^{-1} each for ATLAS and CMS.

JHEP01(2013)069

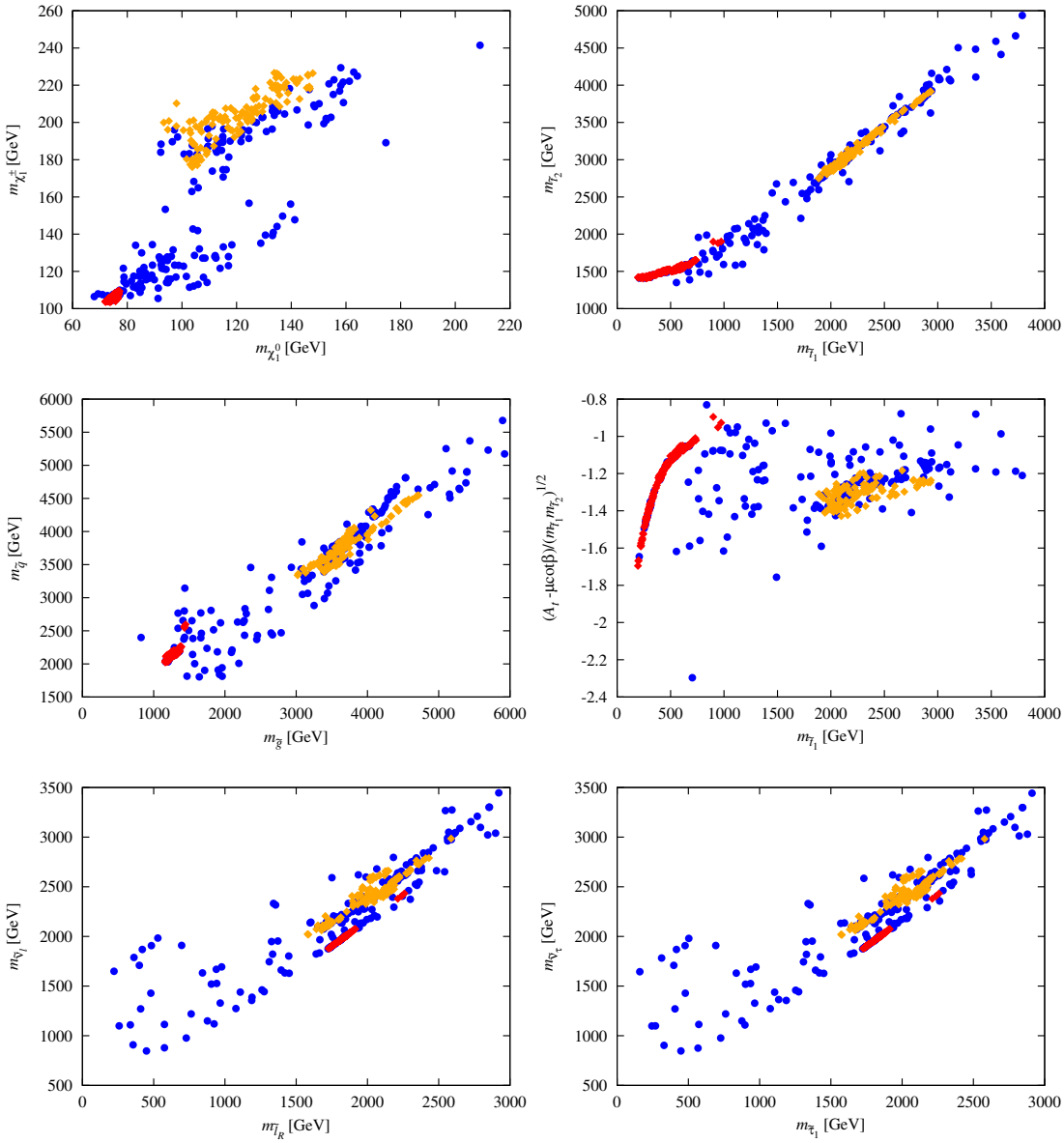

Figure 4. Plots showing $m_{\widetilde{\chi}_1^0}$, $m_{\widetilde{\chi}_1^\pm}$, $m_{\tilde{t}_1}$, $m_{\tilde{t}_2}$, $m_{\tilde{q}}$, $m_{\tilde{g}}$, and the mixing parameter $(A_t - \mu\cot\beta)/\sqrt{m_{\tilde{t}_1} m_{\tilde{t}_2}}$. Also shown are $m_{\widetilde{\ell}_R}$, $m_{\widetilde{\nu}_\ell}$, $m_{\tilde{\tau}_1}$ and $m_{\widetilde{\nu}_\tau}$, where $\ell = e, \mu$.

$m_{h_3} \simeq m_{H^\pm} \simeq m_{a_2}$ for the scenarios considered. We note that small m_{a_1} is typical of the WMAP-window points. We discuss discovery prospects for the a_1 later in the paper. The masses of some crucial SUSY particles are displayed in figure 4. We observe the typically low values of $m_{\widetilde{\chi}_1^0}$ and $m_{\widetilde{\chi}_1^\pm}$, the possibility of $m_{\tilde{t}_1}$ as small as 197 GeV, the mostly modest values of the mixing parameter $(A_t - \mu\cot\beta)/\sqrt{m_{\tilde{t}_1} m_{\tilde{t}_2}}$, and the fact that the predicted $m_{\tilde{q}}$ and $m_{\tilde{g}}$ are beyond current experimental limits, although the lowest values (as found in particular in region A) may soon be probed. Note that $m_{\tilde{g}}$ can be below $m_{\widetilde{\ell}_R}$ (as common in constrained models when m_0 is large) for some points, including the points in region A.

JHEP01(2013)069

Low values of $m_{\widetilde{\chi}_1^0}$ are typical for the scan points, but more particular to this model are the rather low values of $m_{\widetilde{\chi}_1^\pm}$. ATLAS and CMS are currently performing analyses that could in principle be sensitive to the $m_{\widetilde{\chi}_1^\pm}$ values predicted in this model. For some points, $m_{\widetilde{\chi}_1^\pm} - m_{\widetilde{\chi}_1^0}$ can be rather small, implying some difficulty in isolating the leptons or jets associated with $\widetilde{\chi}_1^\pm \to \widetilde{\chi}_1^0 + X$ decays. However, it should be noted that for the WMAP-window points $m_{\widetilde{\chi}_1^\pm} - m_{\widetilde{\chi}_1^0}$ is typically quite substantial, at least 35 GeV for the low-$m_{\widetilde{\chi}_1^0}$ points, so that for these points the above difficulty would not arise. Of particular interest is the very large range of $m_{\tilde{t}_1}$ that arises in the $98 + 125$ GeV LEP-LHC Higgs scenarios. For lighter values of $m_{\tilde{t}_1}$, as typical of the WMAP-window points in region A, the $\tilde{t}_1$ always decays via $\tilde{t}_1 \to \widetilde{\chi}_1^+ b$ or $\tilde{t}_1 \to \widetilde{\chi}_1^0 t$, the latter being absent when $m_{\tilde{t}_1} < m_{\widetilde{\chi}_1^0} + m_t$. At high $m_{\tilde{t}_1}$, these same channels are present but also $\tilde{t}_1 \to \widetilde{\chi}_{2,3,4,5}^0 t$ can be important, which channels being present depending upon whether $m_{\tilde{t}_1} - m_{\chi_{2,3,4,5}^0} - m_t > 0$ or not.

It is interesting to survey the GUT scale parameters that lead to the scenarios of interest. Relevant plots are shown in figure 5. No particular regions of these parameters appear to be singled out aside from some preference for negative values of A_0. These plots show clearly that scenarios A and B correspond to distinct regions in the parameter space. Note however that the density of red points in these plots is purely due to our scan procedures which have some focus on region A.

4 Dark matter, including LSP and light chargino compositions

The composition of the $\widetilde{\chi}_1^0$ and the $\widetilde{\chi}_1^\pm$ are crucial when it comes to the relic density of the $\widetilde{\chi}_1^0$. For those points in the WMAP window in region A (red diamonds), the $\widetilde{\chi}_1^0$ can have a large Higgsino fraction since the $\widetilde{\chi}_1^0\widetilde{\chi}_1^0 \to W^+W^-$ annihilation mode (mainly via t-channel exchange of the light Higgsino-like — see second plot of figure 6 — chargino) is below threshold; the group of points with $m_{\widetilde{\chi}_1^0} > 93$ GeV (region B, orange diamonds) can lie in the WMAP window only if the $\widetilde{\chi}_1^0$ does not have a large Higgsino fraction. This division is clearly seen in figure 6. We note that to a reasonable approximation the singlino fraction of the $\widetilde{\chi}_1^0$ is given by 1 minus the Higgsino fraction plotted in the left-hand window of the figure.

Dark matter (DM) properties for the surviving NMSSM parameter points are summarized in figure 7. Referring to the figure, we see a mixture of blue circle points (those with $\Omega h^2 < 0.094$) and red/orange diamond points (those with $0.094 \leq \Omega h^2 \leq 0.136$, i.e. in the WMAP window). The main mechanism at work to make Ωh^2 too small for many points is rapid $\widetilde{\chi}_1^0\widetilde{\chi}_1^0$ annihilation to W^+W^- due to a substantial Higgsino component of the $\widetilde{\chi}_1^0$ (see third plot of figure 7). Indeed, the relic density of a Higgsino LSP is typically of order $\Omega h^2 \approx 10^{-3} - 10^{-2}$. As the Higgsino component declines Ωh^2 increases and (except for the strongly overlapping points with $m_{\widetilde{\chi}_1^0} < m_W$, for which $\widetilde{\chi}_1^0\widetilde{\chi}_1^0 \to W^+W^-$ is below threshold) it is the points for which the LSP is dominantly singlino that have large enough Ωh^2 to fall in the WMAP window.

Also plotted in figure 7 is the spin-independent direct detection cross section, $\sigma_{\rm SI}$, as a function of $m_{\widetilde{\chi}_1^0}$. First of all, we note that the 2012 XENON100 limits on $\sigma_{\rm SI}$ are obeyed by all the points that have Ωh^2 in the WMAP window, even though our scans

JHEP01(2013)069

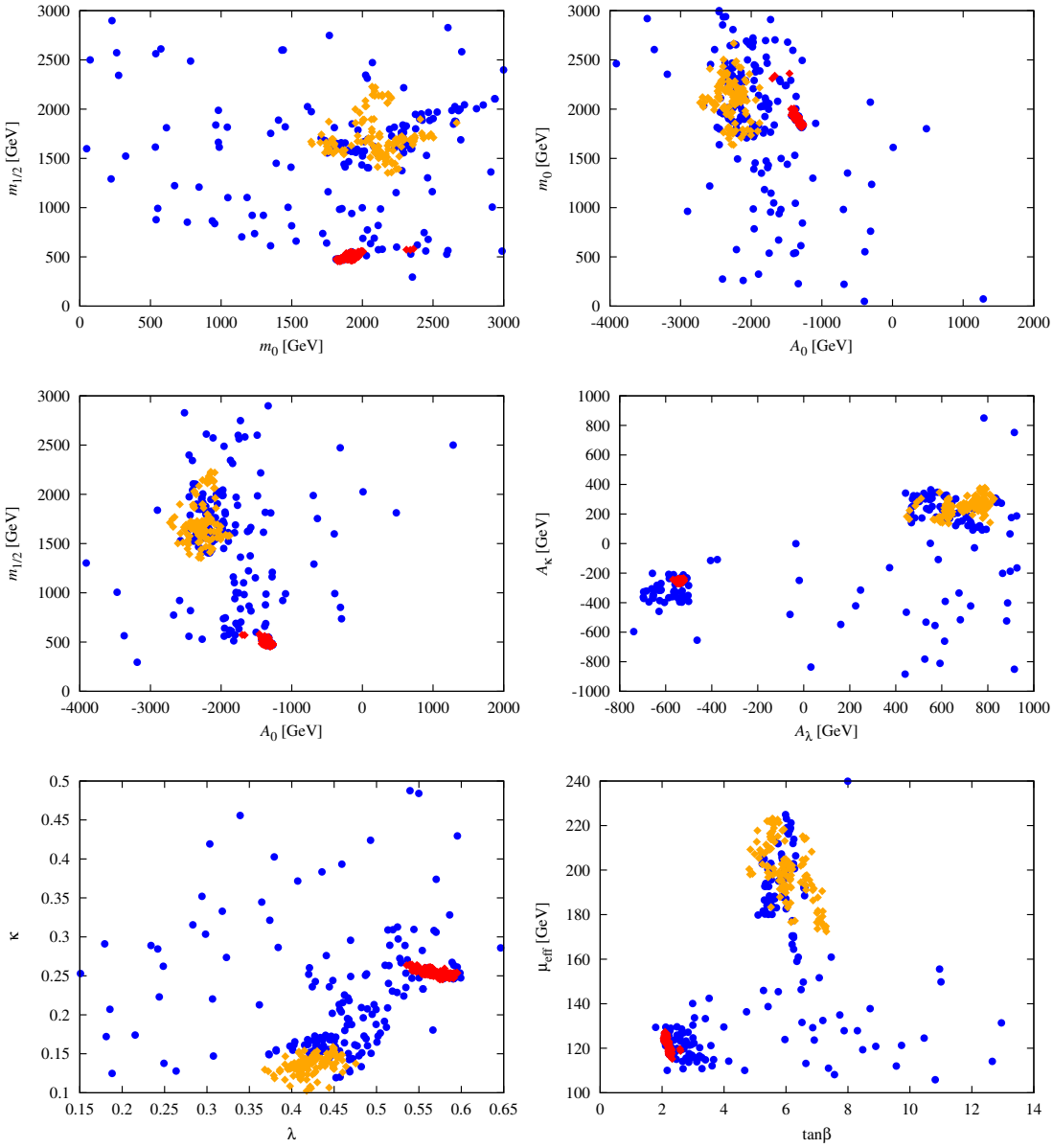

Figure 5. GUT scale and SUSY scale parameters leading to the 98 + 125 GeV LEP-LHC Higgs scenarios.

only implemented the 2011 XENON100 limits — indeed only a modest number of the $\Omega h^2 < 0.094$ points are inconsistent with the 2012 limits. The $\sigma_{\rm SI}$ plot also shows that experiments probing the spin-independent cross section will reach sensitivities that will probe some of the $\sigma_{\rm SI}$ values that survive the 2012 XENON100 limits relatively soon, especially the $m_{\widetilde{\chi}_1^0} > 93$ GeV points that are in the WMAP window (region B). However, it is also noteworthy that the $m_{\widetilde{\chi}_1^0} \sim 75$ GeV points in region A can have very small $\sigma_{\rm SI}$.

The fourth plot of figure 7 and fifth plot of figure 5 illustrate clearly the two categories of WMAP-window points. The first category (A) of points is that for which the $\widetilde{\chi}_1^0$ has

JHEP01(2013)069

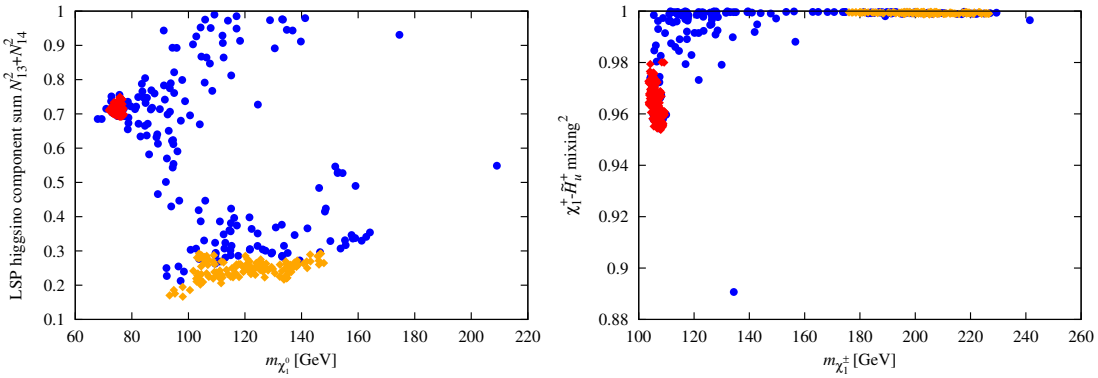

Figure 6. Neutralino and chargino compositions for the 98 + 125 GeV LEP-LHC Higgs scenarios.

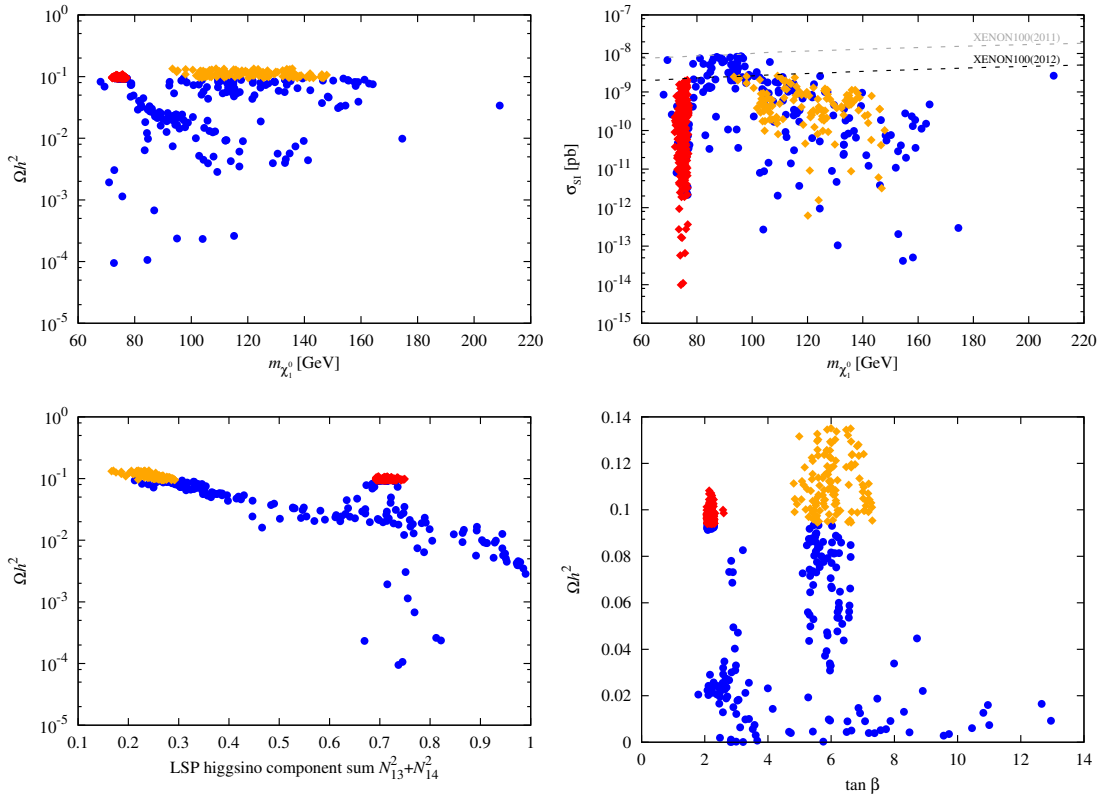

Figure 7. Dark matter properties for the 98 + 125 GeV LEP-LHC Higgs scenarios.

low mass and large Higgsino component with $\tan\beta \in [2, 2.6]$ and $\lambda \in [0.53, 0.6]$; the second category (B) is that for which $m_{\widetilde{\chi}_1^0} > 93$ GeV, $\tan\beta \in [5, 7]$ and $\lambda \in [0.37, 0.48]$.

It is interesting to discuss whether or not any of the 98+125 GeV Higgs scenario points are such as to describe the monochromatic signal at 130 GeV observed in the Fermi-LAT data [18]. We recall that the observation requires $\langle\sigma v\rangle(\widetilde{\chi}_1^0\widetilde{\chi}_1^0 \to \gamma\gamma) \sim 10^{-27}\text{cm}^3/\text{sec}$ (this

JHEP01(2013)069

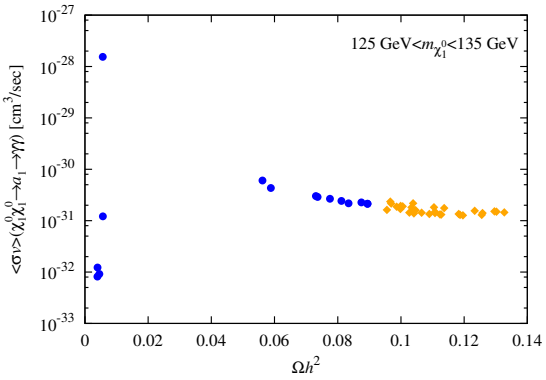

Figure 8. We plot $\langle\sigma v\rangle(\widetilde{\chi}_1^0\widetilde{\chi}_1^0 \to a_1 \to \gamma\gamma)$ vs. Ωh^2 for just those points with $m_{\widetilde{\chi}_1^0} \in [125, 135]$ GeV.

quoted value assumes standard dark matter density, $\rho \sim 0.3$).[5] The situation is illustrated in figure 8 where we plot $\langle\sigma v\rangle(\widetilde{\chi}_1^0\widetilde{\chi}_1^0 \to a_1 \to \gamma\gamma)$ vs. Ωh^2 for just those points with $m_{\widetilde{\chi}_1^0} \in [125, 135]$ GeV. (It is the s-channel a_1 diagram that can give a large $\langle\sigma v\rangle$.) We observe that points with Ωh^2 in the WMAP window have values of $\langle\sigma v\rangle$ four orders of magnitude below that required to explain the excess. Those points with the largest $\langle\sigma v\rangle$ always have quite small Ωh^2 and hence ρ_{DM}. Incidentally, we have checked that all the points in our plots are fully consistent with the current bounds from the continuum γ spectrum as measured by Fermi-LAT [19, 20].

If the 130 GeV gamma ray line is confirmed, then the above questions will need to be explored more carefully. That a fully general NMSSM model (no GUT scale unifications) can be consistent simultaneously with the WMAP window, $\langle\sigma v\rangle(\widetilde{\chi}_1^0\widetilde{\chi}_1^0 \to a_1 \to \gamma\gamma) \sim 10^{-27}\text{cm}^3/\text{sec}$, a Higgs mass close to 125 GeV and 2011 XENON100 constraints was demonstrated in [21]. However, the value of m_{a_1} has to be carefully tuned and the 125 GeV Higgs couplings to all particles (including photons) must be within 5% of those for a SM Higgs boson of this mass, implying difficulty in describing the enhanced $\gamma\gamma$ LHC rates in this channel. Some general (non-NMSSM) theoretical discussions of the 130 GeV line in the context of DM appear in [22, 23].

5 Future tests of the 98+125 GeV Higgs scenario

A critical issue is what other observations would either confirm or rule out the 98+125 GeV LEP-LHC Higgs scenarios. We first discuss possibilities at the LHC and then turn to future colliders, including a future e^+e^- collider, a possible $\gamma\gamma$ collider and a future $\mu^+\mu^-$ collider.

[5] Here, and below, v is the very small velocity typical of dark matter in the current epoch, $v \sim 10^{-3}c$, as relevant for indirect detection of the $\widetilde{\chi}_1^0$ through $\widetilde{\chi}_1^0\widetilde{\chi}_1^0$ annihilations. This, of course, differs from the velocity at the time of freeze out, which is substantially higher.

JHEP01(2013)069

5.1 Direct Higgs production and decay at the LHC

We have already noted in the discussion of figure 2 that gg and VBF production of the h_1 with $h_1 \to b\bar{b}$ provide event rates that might eventually be observable at the LHC once much higher integrated luminosity is attained. Other possibilities include production and decay of the a_1, a_2, and h_3. Decay branching ratios and LHC cross sections in the gg fusion mode for a_1, a_2 and h_3 are shown in figure 9. Since the a_1 is dominantly singlet in nature, its production rates at the LHC are rather small. The largest $\sigma\mathrm{BR}(X)$ values are in the $X = b\bar{b}$ final state, but this final state will have huge backgrounds. When allowed, $\sigma\mathrm{BR}(X)$ for $X = \widetilde{\chi}_1^0\widetilde{\chi}_1^0$ can be significant, but observation of this invisible final state would require a jet or photon tag that would further decrease the cross section. The a_2 is dominantly doublet and provides better discovery prospects. If $m_{a_2} > 2m_t$, the $t\bar{t}$ final state has $\sigma(gg \to a_2)\mathrm{BR}(a_2 \to t\bar{t}) > 0.01$ pb for $m_{a_2} < 550$ GeV, implying > 200 events for $L = 20$ fb^{-1}. A study is needed to determine if this would be observable in the presence of the $t\bar{t}$ continuum background. No doubt, efficient b tagging and reconstruction of the $t\bar{t}$ invariant mass in, say, the single lepton final state would be needed. For $m_{a_2} < 2m_t$, the $X = a_1h_2$ final state with both a_1 and h_2 decaying to $b\bar{b}$ might be visible above backgrounds. However, a dedicated study of this particular decay mode is still lacking. Similar remarks apply in the case of the h_3 where the possibly visible final states are $t\bar{t}$ for $m_{h_3} > 2m_t$ and h_1h_2 for $m_{h_3} < 2m_t$. For both the a_2 and h_3, $\sigma\mathrm{BR}(X)$ is substantial for $X = \widetilde{\chi}_1^0\widetilde{\chi}_1^0$, but to isolate this invisible final state would require an additional photon or jet tag which would reduce the cross section from the level shown.

A final possible detection mode is $gg \to a_2, h_3 \to \tau^+\tau^-$. For this case we plot in figure 10 the effective down-quark coupling, $C_d^{a_2,h_3}(\mathrm{eff})$ vs. m_{a_2} and m_{h_3}, where we define

$$C_d^{a_2,h_3}(\mathrm{eff}) = |C_d^{a_2,h_3}| \left[\frac{\mathrm{BR}(a_2, h_3 \to \tau^+\tau^-)}{0.1}\right]^{1/2} \tag{5.1}$$

and where 0.1 is a reference value of $\mathrm{BR}(H, A \to \tau^+\tau^-)$ implicit in the MSSM limit plots discussed below. Noting that $m_{a_2} \simeq m_{h_3}$ and the fact that the two plots are nearly identical shows that we may sum the a_2 and h_3 signals together in the same manner as the H and A signals are summed together in the case of the analogous plot of $\tan\beta$ vs. $m_A \simeq m_H$ in the case of the MSSM. Limits from CMS 4.6 fb^{-1} data [24] are of order $C_d^{a_2,h_3}(\mathrm{eff}) \lesssim 7-8$ for $m_{a_2} \simeq m_{h_3} \in [150, 220]$ GeV rising rapidly to reach ~ 50 at degenerate mass of order 500 GeV. A dedicated study is needed to determine the precise luminosity for which LHC detection or meaningful limits will become possible for $C_d^{a_2,h_3}(\mathrm{eff}) \lesssim 1$ (as relevant for $m_{a_2}, m_{h_3} < 550$ GeV). Even though Higgs cross sections from gg fusion increase, relative to $\sqrt{s} = 8$ TeV, for $\sqrt{s} = 14$ TeV quite high luminosity will be needed. Currently, for example, the CMS limit from 10 fb^{-1} of data at $m_{a_2} \simeq m_{h_3} \sim 300$ GeV is of order 18, and this amplitude level limit will only improve statistically by $1/L^{1/4}$. Even accounting for the $\sqrt{s} = 14$ TeV cross section increase, very significant improvements in the sensitivity of this analysis will be needed.

The branching ratios for the $H^\pm$ are plotted in figure 11. Prospects for its discovery at masses for which H^+H^- production has substantial cross section appear to be promising

JHEP01(2013)069

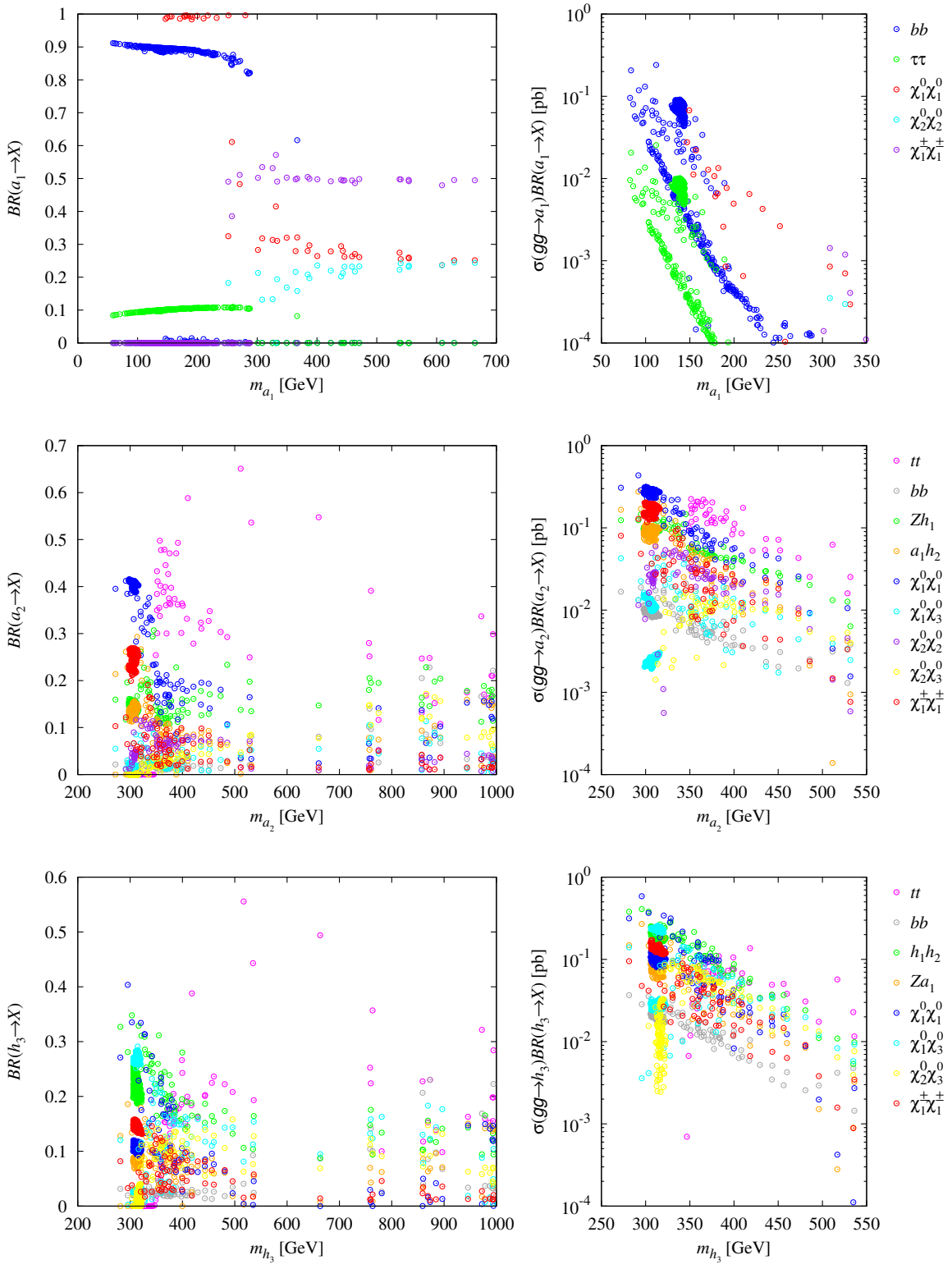

Figure 9. Branching ratios and LHC cross sections in the gg fusion mode (at $\sqrt{s} = 8$ TeV) for a_1, a_2 and h_3.

JHEP01(2013)069

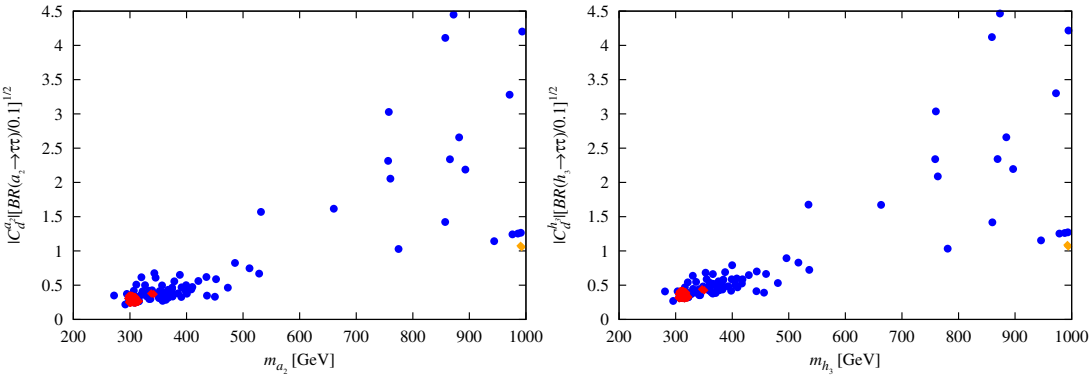

Figure 10. $C_d^{a_2,h_3}$(eff), see eq. (5.1), vs. m_{a_2} and m_{h_3} for $gg \to a_2, h_3 \to \tau^+\tau^-$.

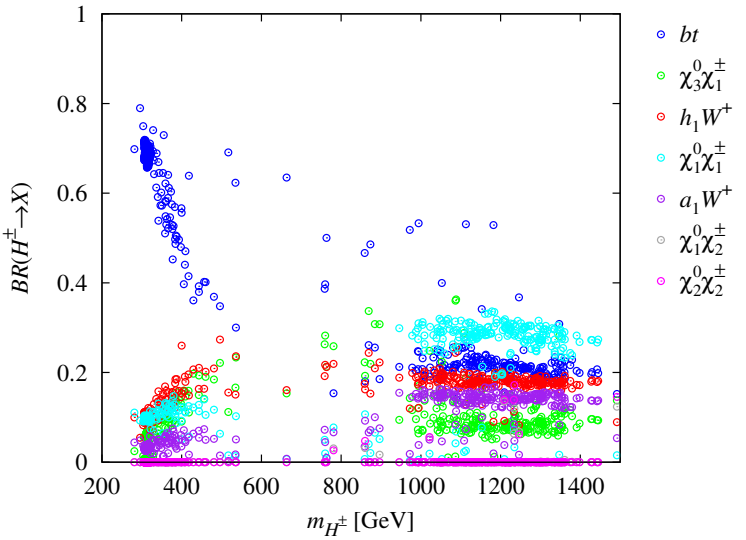

Figure 11. Decay branching ratios of the charged Higgs bosons.

in the bt final state provided reconstruction of the bt mass is possible with good efficiency and one or more b tags are sufficient to reject SM background. Also very interesting would be detection of $H^\pm \to h_1 W^\pm$ in the $h_1 \to b\bar{b}$ final state using mass reconstruction for the $b\bar{b}$ and a leptonic trigger from the $W^\pm$ to reject backgrounds. This channel could prove especially essential in order to detect the $m_{h_1} \sim 98$ GeV Higgs at the LHC and verify the $98 + 125$ GeV Higgs scenario.

5.2 Higgses from neutralino decays

Given that cascades from gluinos/squarks will have low event rate as a result of the large $m_{\tilde{g}}$ and $m_{\tilde{q}}$ masses predicted and the rather low $\widetilde{\chi}_1^\pm$ and $\widetilde{\chi}_1^0$ masses typical of the NMSSM scenarios we discuss, prospects for detecting chargino pair production and neutralino+chargino production would appear to be better, although one is faced with cross sections that are electroweak in size. Of particular interest is whether some of the Higgs

JHEP01(2013)069

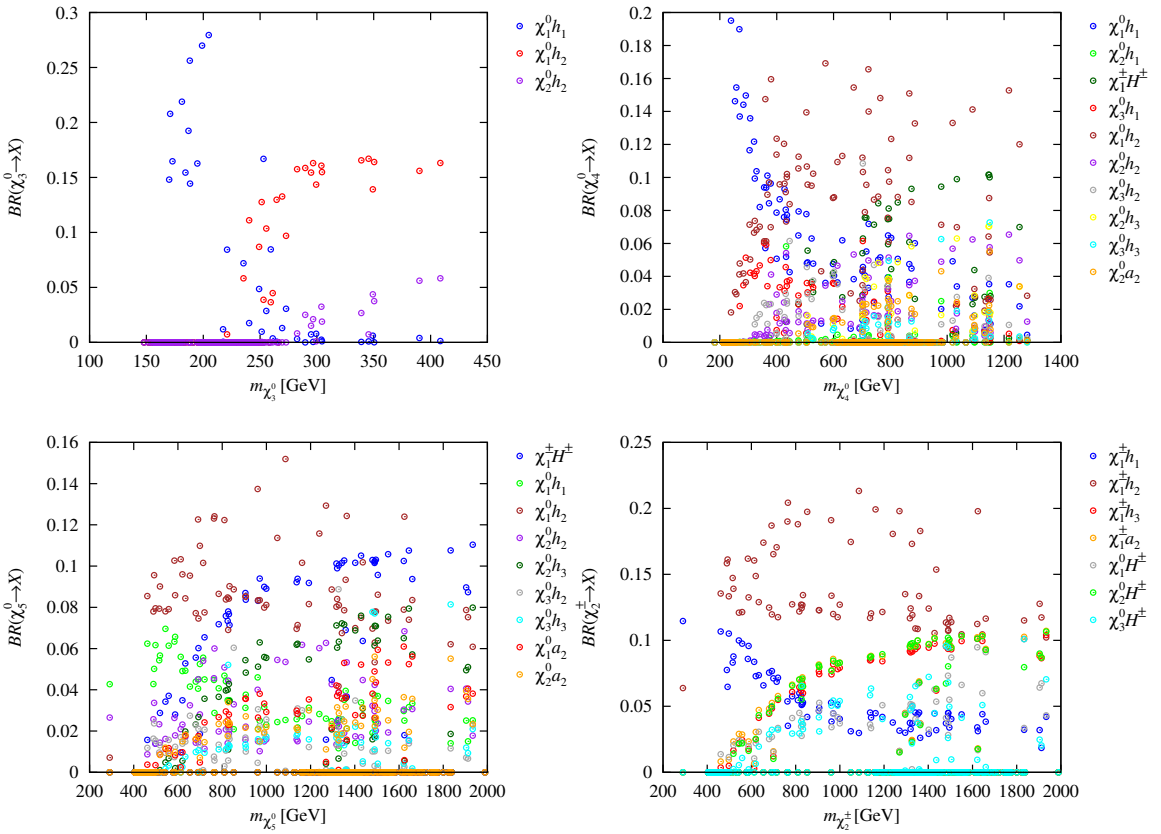

Figure 12. Branching ratios for neutralino and chargino decays into final states containing a Higgs boson for the $98 + 125$ GeV LEP-LHC Higgs scenarios.

bosons can be detected via ino-pair production. To assess the possibilities, we present in figure 12 the branching ratios for the decay of the neutralinos and charginos to lighter inos plus a Higgs boson. A brief summary of the results shown is in order. First, decays to the a_1 are not shown since they have very low branching ratios due to the singlet nature of the a_1. The only decay with branching ratio to the a_2 above 0.1 is $\widetilde{\chi}_2^\pm \to \widetilde{\chi}_1^\pm a_2$ with $m_{\widetilde{\chi}_2^\pm} \gtrsim 1.4$ TeV (beyond LHC reach via electroweak production). In contrast, prospects for the all important h_1 are quite good, with BR$(\widetilde{\chi}_3^0, \widetilde{\chi}_4^0 \to \widetilde{\chi}_1^0 h_1)$ and BR$(\widetilde{\chi}_2^\pm \to \widetilde{\chi}_1^\pm h_1)$ being quite substantial (i.e. > 0.1) at lower values of $m_{\widetilde{\chi}_3^0}, m_{\widetilde{\chi}_4^0}$ and $m_{\widetilde{\chi}_2^\pm}$, respectively. Decays of $\widetilde{\chi}_3^0, \widetilde{\chi}_4^0, \widetilde{\chi}_5^0$ to $\widetilde{\chi}_1^0 h_2$ all have BR > 0.1 once $m_{\widetilde{\chi}_3^0}, m_{\widetilde{\chi}_4^0}, m_{\widetilde{\chi}_5^0}$ are $\gtrsim 250, 400, 500$ GeV, respectively. Similarly, BR$(\widetilde{\chi}_2^\pm \to \widetilde{\chi}_1^\pm h_2) > 0.1$ for $m_{\widetilde{\chi}_2^\pm} \gtrsim 500$ GeV. Since the charged Higgs has $m_{H^\pm} > 300$ GeV, decays to it, although present for the $\widetilde{\chi}_4^0$, $\widetilde{\chi}_5^0$ and $\widetilde{\chi}_2^\pm$, do not have BR > 0.1 until $m_{\widetilde{\chi}_4^0}, m_{\widetilde{\chi}_5^0}, m_{\widetilde{\chi}_2^\pm} \gtrsim 1.1, 1.3, 1.3$ TeV, respectively.

5.3 Linear collider and photon collider tests

An e^+e^- collider would be the ideal machine to produce the additional Higgs states and resolve the scenario. Production cross sections for the various Higgs final states are shown in figure 13 for the three illustrative scenarios specified in table 1 taken from our NMSSM

JHEP01(2013)069

Scenario	m_{h_1}	m_{h_2}	m_{h_3}	m_{a_1}	m_{a_2}	$m_{H^\pm}$	$m_{\widetilde{\chi}_1^0}$	Ωh^2	LSP singlino	LSP Higgsino	$R_{gg}^{h_2}(\gamma\gamma)$
I	99	124	311	140	302	295	76	0.099	18%	75%	1.62
II	97	124	481	217	473	466	92	0.026	20%	74 %	1.53
III	99	126	993	147	991	989	115	0.099	75%	25%	1.14

Table 1. Higgs masses and LSP mass in GeV for the three scenarios for which we plot e^+e^- cross sections in figure 13. Also given are Ωh^2, the singlino and Higgsino percentages and $R_{gg}^{h_2}(\gamma\gamma)$. Scenarios I) and III) have Ωh^2 in the WMAP window, with I) being typical of the low-$m_{\widetilde{\chi}_1^0}$ scenarios and III) being that with smallest m_{h_3} in the large-$m_{\widetilde{\chi}_1^0}$ group of points in the WMAP window. Scenario II) is chosen to have m_{a_2} and m_{h_3} intermediate between those for scenario I) and III), a region for which Ωh^2 is substantially below 0.1.

scans. The first plot is for a WMAP-window scenario with $m_{\widetilde{\chi}_1^0} \sim 76$ GeV and light Higgs bosons. The third plot is for the point in region B with smallest m_{h_3}, for which $m_{a_2}, m_{h_3}, m_{H^\pm}$ are all around 1 TeV. The second plot is for a sample scenario with Higgs masses that are intermediate, as only possible if Ωh^2 lies below the WMAP window. With an integrated luminosity of 1000 fb^{-1}, substantial event rates for many Z+Higgs and Higgs pair final states are predicted. Of course, Zh_1 and Zh_2 production have the largest cross sections and lowest thresholds. The next lowest thresholds are for a_1h_1 production, but the cross sections are quite small, $< 0.1, 0.01, 0.001$ fb, respectively. The a_1h_2 cross sections are even smaller. Next in line are a_1h_3, a_2h_1 and a_2h_2, with a_2h_1 having thresholds $> 400, 600, 1190$ GeV for scenarios I), II) and III), respectively, as well as having the largest cross section, peaking at $\sigma > 0.7, 0.2, 0.007$ fb for the three respective scenarios. Production of a_2h_3 and H^+H^- have thresholds $> 620, 950, 2000$ GeV, respectively, but have much larger cross sections, that for H^+H^- being $> 16.6, 6.3, 1.4$ fb at the peak, for the three respective scenarios.

In the e^+e^- collider case, it would be easy to isolate signals in many final states. For example, in the case of Higgs pairs, final states such as $(t\bar{t})(t\bar{t})$, $(\widetilde{\chi}_1^0\widetilde{\chi}_1^0)(t\bar{t})$ and so forth could be readily identified above background. Observation of the $(\widetilde{\chi}_1^0\widetilde{\chi}_1^0)(\widetilde{\chi}_1^0\widetilde{\chi}_1^0)$ final states would require a photon tag and would thus suffer from a reduced cross section. Associated Z+Higgs, with Higgs decaying to $t\bar{t}$ or $\widetilde{\chi}_1^0\widetilde{\chi}_1^0$ would be even more readily observed.

Another future collider that would become possible if an e^+e^- (or e^-e^-) collider is built is a $\gamma\gamma$ collider where the γ's are obtained by backscattering of laser photons off the energetic e's. For a recent summary see [25] and references therein. A huge range of energies is possible for such a $\gamma\gamma$ collider, ranging from low to high center of mass energies depending upon the center of mass energy of the underlying electron collider. A $\gamma\gamma$ collider based on e^-e^- collisions can even be considered as a stand-alone machine that could be built before an e^+e^- collider, especially if high $\sqrt{s}_{\gamma\gamma}$ is not needed. Typically, the largest $\sqrt{s}_{\gamma\gamma}$ that is possible with large instantaneous $\gamma\gamma$ luminosity is of order $0.8\sqrt{s}_{e^+e^-}$. That $\gamma\gamma \to$Higgs is an effective way to study a SM Higgs boson has been well established [26–28]. For low Higgs masses, the required electron collider could have energy of order $m_{\rm Higgs}/0.8$.

In the present context, it is of interest to assess the extent to which a $\gamma\gamma$ collider would be able to study the neutral NMSSM Higgs bosons. This is determined by the

JHEP01(2013)069

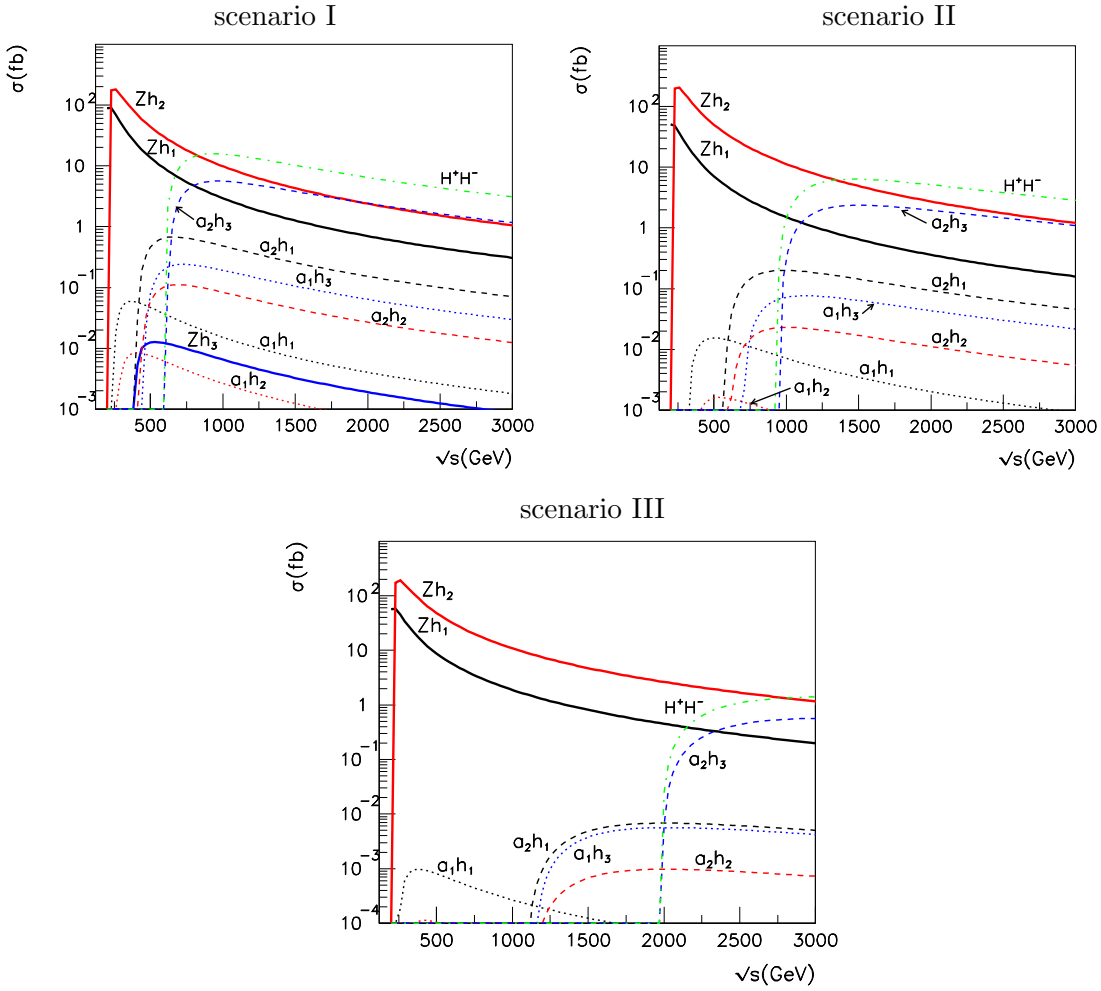

Figure 13. Cross sections for Higgs production at an e^+e^- collider, as functions of the center-of-mass energy $\sqrt{s}$, for three illustrative mass spectra as tabulated in table 1.

ratio of the $\gamma\gamma$ coupling squared of the given Higgs boson to that of the SM Higgs. In figure 14 we present plots of $(C^h_{\gamma\gamma})^2$ as a function of m_h for $h = h_1, h_2, h_3, a_1, a_2$ for masses below 1 TeV. The fairly SM-like h_2 at ~ 125 GeV can be studied easily at such a collider since its $\gamma\gamma$ coupling is close to SM strength. For example, at an e^-e^- collider with the optimal $E_{ee} = 206$ GeV, a 125 GeV SM Higgs has a cross section of 200 fb. After two years of operation, equivalent to $L = 500$ fb^{-1}, one can measure the $b\bar{b}, W^+W^-, \gamma\gamma$ partial widths with accuracies of $\Delta\Gamma(b\bar{b}, W^+W^-, \gamma\gamma)/\Gamma(b\bar{b}, W^+W^-, \gamma\gamma) \sim 0.015, 0.04, 0.06$, respectively [27] (see also [26, 28]).

Even though the h_1 and a_1 are largely singlet, both have $\gamma\gamma$ couplings-squared that are often of order 0.1×SM and above (at the same mass). In part, this is because even singlets couple to $\gamma\gamma$ through a Higgsino-like chargino loop using the singlet-Higgsino-Higgsino coupling that arises from the $\lambda\widehat{S}\widehat{H}_u\widehat{H}_d$ term in the superpotential. Indeed, this coupling becomes stronger as λ is increased. Of course, it is important to note that the

JHEP01(2013)069

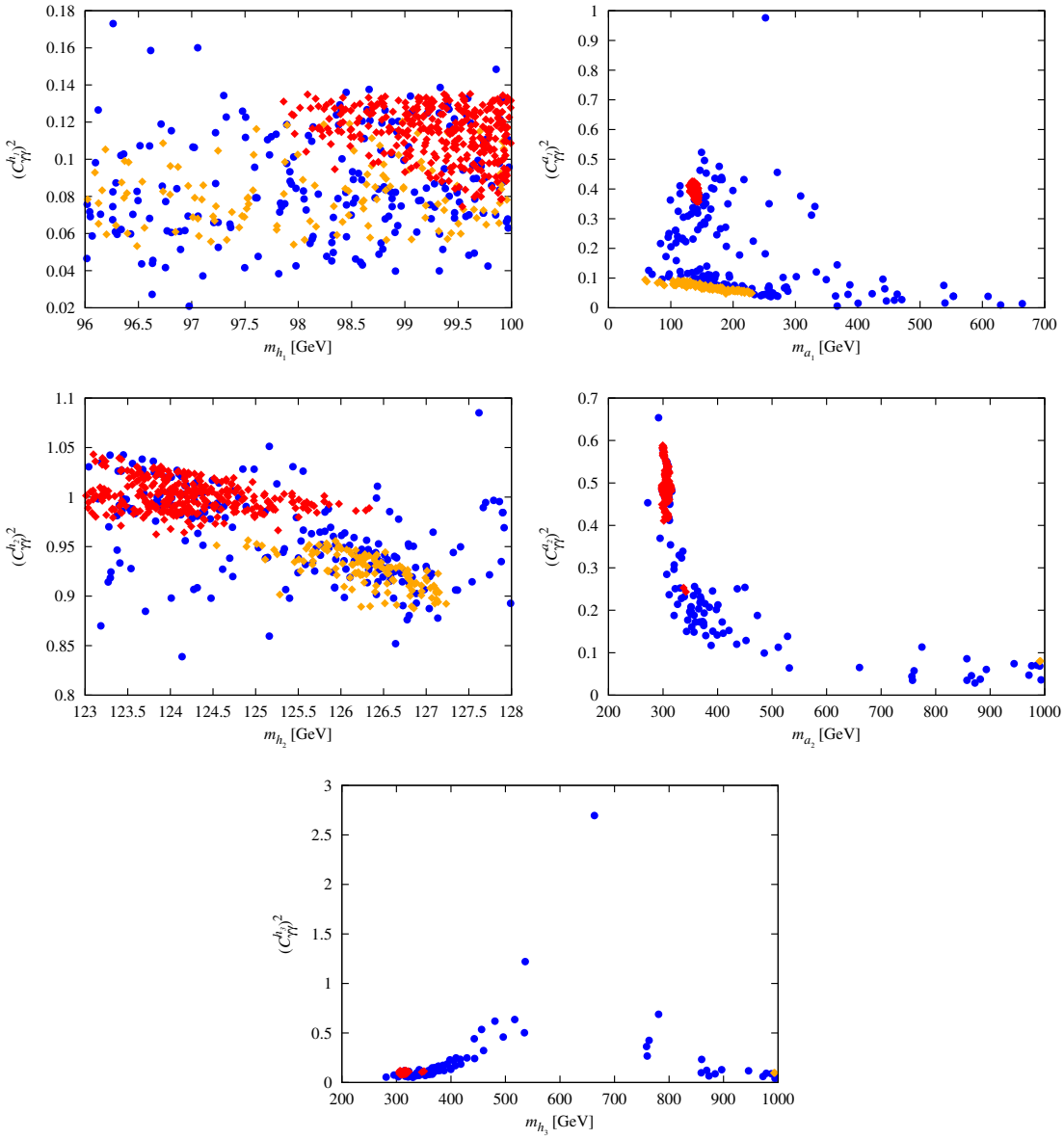

Figure 14. $(C^h_{\gamma\gamma})^2$ as a function of m_h for $h = h_1, h_2, h_3, a_1, a_2$.

modest values of $\mu_{\rm eff}$ (see figure 5) that characterize many of our scenarios imply that the lightest chargino is largely Higgsino-like and has low mass (see figure 6), for which the Higgsino-chargino loop is less suppressed. Even for $\gamma\gamma$ coupling-squared of order 0.1×SM, with sufficient integrated luminosity observation of the h_1 and a_1 would be possible. For example, for suitably chosen E_{ee}, the above SM Higgs rates multiplied by 0.1 would roughly apply for $m_{h_1} \sim 98$ GeV or $m_{a_1} < 300$ GeV, from which it is clear that the $b\bar{b}$ final state would be easily observable with $L = 500$ fb^{-1} and one could measure the partial width with an accuracy of order 5%. Even the h_3 and a_2 would be observable for $m_{a_2} < 500$ GeV, again assuming appropriately optimal E_{ee} for the given m_{h_3} or m_{a_2} and $L = 500$ fb^{-1}.

JHEP01(2013)069

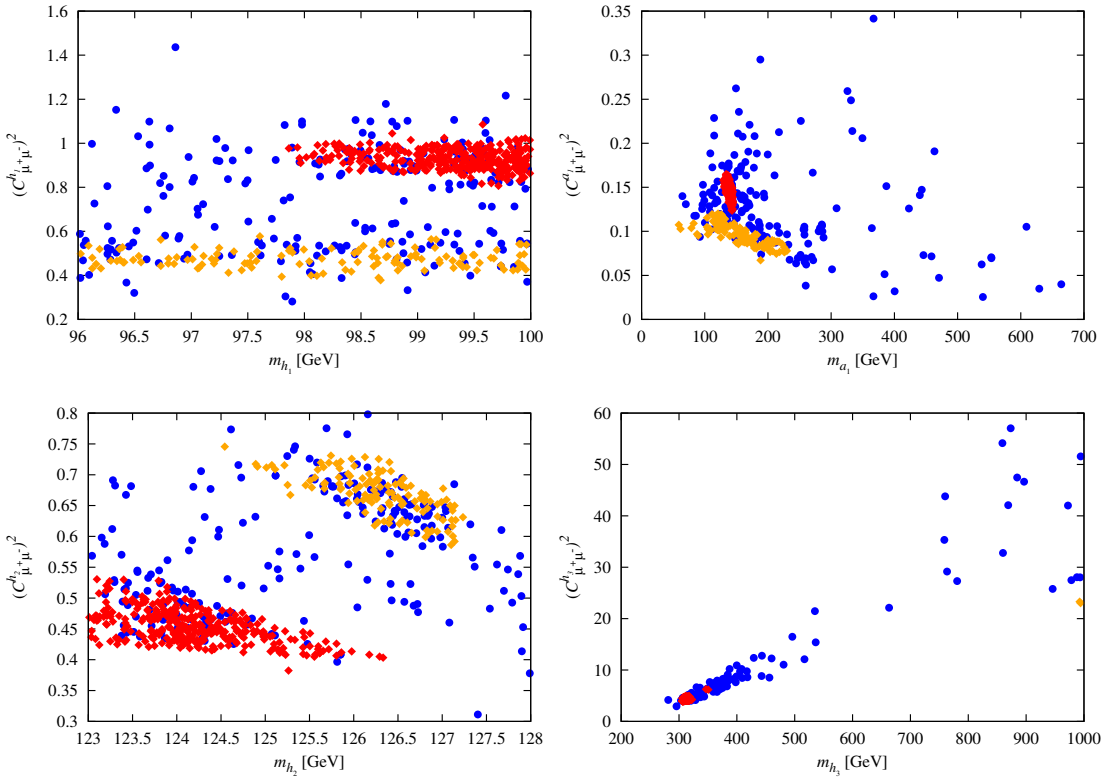

Figure 15. Reduced $\mu^+\mu^-$ couplings squared for h_1, h_2, h_3, a_1.

This raises the question of whether or not a $\gamma\gamma$ collider with adjustable (as is straightforward) $\sqrt{s}_{\gamma\gamma}$ in the 98 GeV range would be a good next step for high energy physics. It would have the advantage of allowing important detailed studies of the h_2 (or any SM-like Higgs boson with mass of 125 GeV) while testing for the presence of the h_1. With adjustable $\sqrt{s}_{\gamma\gamma}$ and $L \geq 500$ fb^{-1}, the h_3, a_1, a_2, or any other light Higgs boson with significant (even if somewhat suppressed) $\gamma\gamma$ coupling, would be observable as well.

5.4 A $\mu^+\mu^-$ collider

A muon-collider with $\sqrt{s}$ close to the Higgs mass in question would be a particularly ideal machine to study any Higgs boson with $\mu^+\mu^-$ coupling that is not too different from that of a SM Higgs boson of similar mass. Thus, in figure 15 we present plots of $(C^h_{\mu^+\mu^-})^2$ as a function of m_h for $h = h_1, h_2, h_3, a_1$, that for the a_2 being essentially identical to the $h = h_3$ case. We see that prospects are really quite good for the h_1 as well as the h_2. In addition, the WMAP-window a_1 points, all of which lie at relatively low mass, can be probed as well. As for the h_3 (and the a_2), the low-$m_{\widetilde{\chi}^0_1}$ region points with low m_{h_3} (and low m_{a_2}) have nicely enhanced $(C^{h_3}_{\mu^+\mu^-})^2$ (and $(C^{h_3}_{\mu^+\mu^-})^2$). A muon collider would be ideal for probing such scenarios. Additional experimental evidence for this $98 + 125$ GeV Higgs scenario from other machines would provide strong motivation for the muon collider.

JHEP01(2013)069

6 Conclusions

To summarize, we have emphasized the possibility that both the LEP excess in the $b\bar{b}$ final state at $M_{b\bar{b}} \sim 98$ GeV and the LHC Higgs-like signal at ~ 125 GeV with an enhanced rate in the two-photon final state can be explained in the context of the NMSSM. The NMSSM scenarios of this type have many attractive features. We have particularly emphasized the fact that the h_1 could eventually be observed at the LHC in $gg, \mathrm{VBF} \to h_1 \to b\bar{b}$. We urge the ATLAS and CMS collaborations to give attention to this possibility.

The $98 + 125$ GeV Higgs scenarios have important implications for the other Higgs bosons and for supersymmetric particles. If we focus only on the subset of these scenarios that have relic density in the WMAP window, then there are two separate regions of NMSSM parameter space that emerge. One region (A) is characterized by small $m_{\widetilde{\chi}_1^0} \sim 75$ GeV and low masses for many of the Higgs bosons and superpartners, including $m_{\tilde{t}_1}$ as low as 197 GeV. The second region (B) is characterized by larger $m_{\widetilde{\chi}_1^0} \in [93, 150]$ GeV and much larger mass scales for the heavier Higgs bosons and supersymmetric particles. For this latter region, one finds $m_{a_1} \in [100, 200]$ GeV, $m_{\widetilde{\chi}_1^\pm} \in [170, 230]$ GeV, $m_{a_2} \simeq m_{h_3} \simeq m_{H^\pm} \in [1, 1.4]$ TeV, $m_{\tilde{t}_1} \in [1.9, 2.8]$ TeV, $m_{\tilde{q}}, m_{\tilde{g}} \in [3, 5]$ TeV and $\tan\beta \in [5, 7]$. Clearly this latter region leaves little hope for LHC detection of the colored particles and experimental probes would need to focus on the gauginos and lighter Higgs bosons. It is further associated with rather modest values for the enhancement of the 125 GeV Higgs signal in the $\gamma\gamma$ channel. Information related to the prospects for Higgs and superparticle detection for the two regions (A) and (B) at an e^+e^-, $\gamma\gamma$ or $\mu^+\mu^-$ collider are summarized.

Acknowledgments

The work of JFG and YJ was supported by US DOE grant DE-FG03-91ER40674, that of JHS the U.S. DOE grant No. DE-FG03-92-ER40701, and that of SK and GB by IN2P3 under contract PICS FR–U.S.A. No. 5872. UE acknowledges partial support from the French ANR LFV-CPV-LHC, ANR STR-COSMO and the European Union FP7 ITN INVISIBLES (Marie Curie Actions, PITN-GA-2011-289442). GB, UE, JFG, SK, and JHS acknowledge the hospitality and the inspiring working atmosphere of the Aspen Center for Physics which is supported by the National Science Foundation Grant No. PHY-1066293.

References

[1] ATLAS collaboration, *Observation of a new particle in the search for the Standard Model Higgs boson with the ATLAS detector at the LHC*, *Phys. Lett.* **B 716** (2012) 1 [arXiv:1207.7214] [INSPIRE].

[2] CMS collaboration, *Observation of a new boson at a mass of 125 GeV with the CMS experiment at the LHC*, *Phys. Lett.* **B 716** (2012) 30 [arXiv:1207.7235] [INSPIRE].

JHEP01(2013)069

[3] CDF, D0 collaborations, T. Aaltonen et al., *Evidence for a particle produced in association with weak bosons and decaying to a bottom-antibottom quark pair in Higgs boson searches at the Tevatron*, *Phys. Rev. Lett.* **109** (2012) 071804 [arXiv:1207.6436] [INSPIRE].

[4] M.S. Carena, S. Heinemeyer, C. Wagner and G. Weiglein, *Suggestions for benchmark scenarios for MSSM Higgs boson searches at hadron colliders*, *Eur. Phys. J.* **C 26** (2003) 601 [hep-ph/0202167] [INSPIRE].

[5] U. Ellwanger, *A Higgs boson near 125 GeV with enhanced di-photon signal in the NMSSM*, *JHEP* **03** (2012) 044 [arXiv:1112.3548] [INSPIRE].

[6] J.-J. Cao, Z.-X. Heng, J.M. Yang, Y.-M. Zhang and J.-Y. Zhu, *A SM-like Higgs near 125 GeV in low energy SUSY: a comparative study for MSSM and NMSSM*, *JHEP* **03** (2012) 086 [arXiv:1202.5821] [INSPIRE].

[7] U. Ellwanger and C. Hugonie, *Higgs bosons near 125 GeV in the NMSSM with constraints at the GUT scale*, *Adv. High Energy Phys.* **2012** (2012) 625389 [arXiv:1203.5048] [INSPIRE].

[8] J.F. Gunion, Y. Jiang and S. Kraml, *Could two NMSSM Higgs bosons be present near 125 GeV?*, *Phys. Rev.* **D 86** (2012) 071702 [arXiv:1207.1545] [INSPIRE].

[9] J. Cao, Z. Heng, J.M. Yang and J. Zhu, *Status of low energy SUSY models confronted with the LHC 125 GeV Higgs data*, *JHEP* **10** (2012) 079 [arXiv:1207.3698] [INSPIRE].

[10] ALEPH, DELPHI, L3, OPAL, LEP Working Group for Higgs Boson Searches collaborations, S. Schael et al., *Search for neutral MSSM Higgs bosons at LEP*, *Eur. Phys. J.* **C 47** (2006) 547 [hep-ex/0602042] [INSPIRE].

[11] LEP Working Group for Higgs boson searches, ALEPH, DELPHI, L3, OPAL collaborations, R. Barate et al., *Search for the standard model Higgs boson at LEP*, *Phys. Lett.* **B 565** (2003) 61 [hep-ex/0306033] [INSPIRE].

[12] U. Ellwanger, C. Hugonie and A.M. Teixeira, *The Next-to-Minimal Supersymmetric Standard Model*, *Phys. Rept.* **496** (2010) 1 [arXiv:0910.1785] [INSPIRE].

[13] U. Ellwanger, J.F. Gunion and C. Hugonie, *NMHDECAY: A Fortran code for the Higgs masses, couplings and decay widths in the NMSSM*, *JHEP* **02** (2005) 066 [hep-ph/0406215] [INSPIRE].

[14] U. Ellwanger and C. Hugonie, *NMHDECAY 2.0: An Updated program for sparticle masses, Higgs masses, couplings and decay widths in the NMSSM*, *Comput. Phys. Commun.* **175** (2006) 290 [hep-ph/0508022] [INSPIRE].

[15] *NMSSMTools. Tools for the calculation of the higgs and sparticle spectrum in the NMSSM: NMHDECAY, NMSPEC and NMGMSB*, http://www.th.u-psud.fr/NMHDECAY/nmssmtools.html.

[16] New (g-2) collaboration, F. Gray, *Measuring the muon's anomalous magnetic moment to 0.14 ppm*, *J. Phys. Conf. Ser.* **312** (2011) 102006 [arXiv:1009.0799] [INSPIRE].

[17] J.F. Gunion, Y. Jiang and S. Kraml, *The Constrained NMSSM and Higgs near 125 GeV*, *Phys. Lett.* **B 710** (2012) 454 [arXiv:1201.0982] [INSPIRE].

[18] C. Weniger, *A Tentative Gamma-Ray Line from Dark Matter Annihilation at the Fermi Large Area Telescope*, *JCAP* **08** (2012) 007 [arXiv:1204.2797] [INSPIRE].

[19] LAT collaboration, W. Atwood et al., *The Large Area Telescope on the Fermi Gamma-ray Space Telescope Mission*, *Astrophys. J.* **697** (2009) 1071 [arXiv:0902.1089] [INSPIRE].

JHEP01(2013)069

[20] T. Bringmann, X. Huang, A. Ibarra, S. Vogl and C. Weniger, *Fermi LAT Search for Internal Bremsstrahlung Signatures from Dark Matter Annihilation*, *JCAP* **07** (2012) 054 [arXiv:1203.1312] [INSPIRE].

[21] D. Das, U. Ellwanger and P. Mitropoulos, *A 130 GeV photon line from dark matter annihilation in the NMSSM*, *JCAP* **08** (2012) 003 [arXiv:1206.2639] [INSPIRE].

[22] Y. Bai and J. Shelton, *Gamma Lines without a Continuum: Thermal Models for the Fermi-LAT 130 GeV Gamma Line*, *JHEP* **12** (2012) 056 [arXiv:1208.4100] [INSPIRE].

[23] T. Bringmann and C. Weniger, *Gamma Ray Signals from Dark Matter: Concepts, Status and Prospects*, *Phys. Dark Univ.* **1** (2012) 194 [arXiv:1208.5481] [INSPIRE].

[24] CMS collaboration, *Search for neutral Higgs bosons decaying to τ pairs in pp collisions at $\sqrt{s} = 7$ TeV*, *Phys. Lett.* **B 713** (2012) 68 [arXiv:1202.4083] [INSPIRE].

[25] J. Gronberg, *Photon Linear Collider Gamma-Gamma Summary*, arXiv:1203.0031 [INSPIRE].

[26] D.M. Asner, J.B. Gronberg and J.F. Gunion, *Detecting and studying Higgs bosons at a photon-photon collider*, *Phys. Rev.* **D 67** (2003) 035009 [hep-ph/0110320] [INSPIRE].

[27] M.M. Velasco et al., *Photon photon and electron photon colliders with energies below a TeV*, *eConf* **C 010630** (2001) E3005 [hep-ex/0111055] [INSPIRE].

[28] D. Asner et al., *Complementarity of a low-energy photon collider and LHC physics*, hep-ph/0308103 [INSPIRE].

JHEP01(2013)069